Enhancement of upconversion luminescence of $YAlO_3$: Er^{3+} by Gd^{3+} doping

Zhenlong Li (李振龙)[1], Baoshu Wang (王宝树)[1], Licheng Xing (邢立成)[1], Shaolong Liu (刘绍龙)[1], Na Tan (谭 娜)[1], Siguo Xiao (肖思国)[1,2], and Jianwen Ding (丁建文)[1,2*]

[1]*Department of Physics and Institute for Nanophysics and Rare-earth Luminescence, Xiangtan University, Xiangtan 411105, China*

[2]*Key Laboratory of Low Dimensional Materials & Application Technology, Xiangtan University, Xiangtan 411105, China*

[*]*Corresponding author: jwding@xtu.edu.cn*

Received December 19, 2011; accepted February 24, 2012; posted online April 20, 2012

The upconversion luminescences of $YAlO_3$:Er^{3+} phosphor co-doping with different Gd^{3+} concentrations are investigated under the excitation of 980- and 532-nm diode lasers. A near ultraviolet upconversion emission at 410 nm is observed in $YAlO_3$ under 532-nm excitation. Moreover, the inactive Gd^{3+} ions can improve the upconversion intensity efficiently in a certain range of concentration. Under 980-nm excitation, the visible upconversion emissions at 546 and 646 nm are enhanced by about 10 and 8 times at the Gd^{3+} concentration of 40%, respectively. The upconversion emission at 410 nm under 532-nm excitation is also enhanced by 7 times. The substitution of Gd^{3+} ions for Y^{3+} sites changes the local symmetry of Er^{3+}, leading to the improvement of upconversion efficiency.

OCIS codes: 160.5690, 160.4670, 160.4760.

doi: 10.3788/COL201210.081602.

In the last several decades, the upconversion luminescence of rare-earth-ion-doped materials has been investigated extensively due to their wide applications in solid-state lasers, flat panel displays, biological labeling, and so on[1−3]. Er^{3+} has been reported as one of the most popular and efficient ions for upconversion[4−8]. It can provide several intermediate levels with long life time, which can be directly pumped by several diode lights[9−14].

Recently, upconversion phenomena in Er^{3+}-doped $YAlO_3$ crystals have been widely studied because of their high mechanical hardness and considerable thermal conductivity, among others. Several authors have reported upconversion luminescence in Er^{3+}-doped $YAlO_3$ under 518-, 542.4-, 548.9-, 652.2-, and 980-nm excitations[10,15−17]. Therefore, it is very important to improve their upconversion efficiency. There are many factors affecting the upconversion efficiency, such as the local environment, the dopant concentration, and the distribution of active ions in host materials[18]. A recent study has reported that the luminescence intensity can be enhanced by changing the local environment of luminescent centers, which can be performed by doping some suitable inactive ions in the host. For instance, co-doping with Li^+-Zn^{2+} can prolong the lifetime of the intermediate state $^4I_{11/2}$ of Er^{3+} in Y_2O_3 nanocrystals[19] and enhance the intensity of its upconversion. The presence of Y^{3+} in ZrO_2, which is presumed to reduce concentration quenching, increases the upconversion luminescence intensity of ZrO_2:Er^{3+}[20]. In TeO_2:Tm^{3+}, Yb^{3+}, the blue emission is also increased distinctly with an addition of $BiCl_3$, which is ascribed to the effect of local environment of Tm^{3+} due to the replacement of TeO_2 by $BiCl_3$[21]. This means that co-doping inactive ions may be an efficient way to obtain an enhancement of upconversion efficiency.

In this letter, the enhancement of the upconversion $YAlO_3$:Er^{3+} is reported by the introduction of Gd^{3+} under both 980- and 532-nm excitations. The upconversion mechanism, Gd^{3+}-dependent upconversion behavior, and the local symmetry of Er^{3+} influenced by Gd^{3+} are investigated.

Er^{3+} and Gd^{3+} co-doped $YAlO_3$ with the composition of $Y_{(1-0.05-x)}AlO_3$: 0.05 Er^{3+}, xGd^{3+}(x=0, 0.15, 0.25, 0.4, 0.5, and 0.7) was prepared through a solution combustion synthesis procedure. An aqueous solution containing citric acid, $Y(NO_3)_3$, $Er(NO_3)_3$, and $Gd(NO_3)_3$ was used to synthesize the Er^{3+} and Gd^{3+} co-doped $YAlO_3$ powders. A citric acid-to-metal nitrate molar ratio of 1.5:1 was employed to prepare the precursor solution. After the combustion, the precursor was calcined at 1 100 °C for 2 h.

The powders were characterized by X-ray diffraction (XRD) on a Bruker D8 advanced equipment (x) using Cu tube with K_α radiation of 0.15406 nm in the 2θ range of 20°–60°. The morphology of the prepared powders was observed by scanning electron microscopy (SEM) using JSM-6610. Upconversion luminescence spectra excited by 980- and 532-nm lasers were obtained in the spectrophotometer (R-500, Japan Spectroscopic Co., Japan). All the measurements were performed at room temperature.

Figure 1 shows the representative XRD pattern and the unit cell parameters b and c of the $Y_{0.95-x}Gd_xEr_{0.05}AlO_3$ sample with x (x=0, 0.15, 0.4, 0.5, and 0.75). From Fig. 1(a), the XRD pattern shows that all the samples are synthesized into a typical orthorhombic crystal phase, in accordance with the standard XRD JCPDS 33-0041. The cell parameters b and c of the samples are calculated in terms of the XRD data (see Fig. 1(b)). Given that the ionic radius of Gd^{3+} (0.1193 nm) is bigger than that of Y^{3+} (0.1159 nm), the unit cell parameters b and

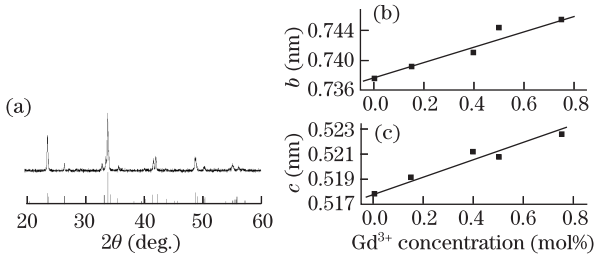

Fig. 1. (a) Representative XRD patterns of $Y_{0.95-x}Gd_xEr_{0.05}AlO_3$ and pure $YAlO_3$ and the concentration dependence of unit cell parameters (b) b and (c) c of $Y_{0.95-x}Gd_xEr_{0.05}AlO_3$ (x=0, 0.15, 0.4, 0.5, and 0.75).

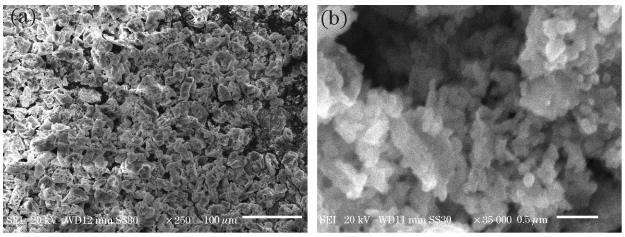

Fig. 2. SEM images for the morphology of the samples at scale bar (a) 100 and (b) 0.5 μm.

c increase linearly with the increase of Gd^{3+} concentration, following Vegard's rule[22]. Figure 2 displays a typical SEM image of the prepared samples. The sample possesses a microstructure of a network with large pores, which is attributed to precursor made by combustion method (see Fig. 2(a)). During the combustion process, a large amount of decomposed gases is formed which break the interconnected particles. The magnified SEM image is shown in Fig. 2(b).

Figure 3 shows the upconversion emission spectra of $Y_{(0.95-x)}AlO_3$: 5 mol% Er^{3+}, x mol% Gd^{3+} under excitations of (a) 980 and (b) 532 nm. Under the excitation of 980 nm, two strong emission bands approximately centered at 550 and 646 nm, respectively, are observed and can each be assigned to the $^2H_{11/2}$/ $^4S_{3/2}$ $\rightarrow ^4I_{15/2}$ and $^4F_{9/2}$ $\rightarrow ^4I_{15/2}$ of Er^{3+} transitions. Three emission bands centered at 410, 655, and 850 nm, respectively, are obtained under 532-nm excitation; these correspond to the transitions of Er^{3+}: $^2G_{9/2}$ $\rightarrow ^4I_{15/2}$, $^4F_{9/2}$ $\rightarrow ^4I_{15/2}$, and $^4I_{9/2}$ $\rightarrow ^4I_{15/2}$, respectively. The abundant upconversion emissions in the ultraviolet range are not obtained in this work[10,15,16]. Only the upconversion emission centered at 410 nm is observed, which may have resulted from a weak absorption at 532 nm in YA1O_3: Er^{3+}[23].

Figure 4 describes schematically the possible upconversion processes in energy level diagrams of Er^{3+} under 980- and 532-nm excitations.

Under the 980 nm excitation, the green emission at 550 nm is performed by the excited state absorption (ESA) and the energy transfer upconversion (ETU). In ESA, the ions in the ground state ($^4I_{15/2}$) absorb a 980-nm laser photon, which is excited to the intermediate $^4I_{11/2}$ state. The same laser pumps the excited ion from the $^4I_{11/2}$ to $^4F_{7/2}$ states. Subsequently, nonradiative relaxation populates the $^4S_{3/2}$ or $^2H_{11/2}$ level. The ETU process occurs between two Er^{3+} ions at the $^4I_{11/2}$ level excited by 980-nm photons. An Er^{3+} ion at the $^4I_{11/2}$ state relaxes to the ground state, transferring its energy to another Er^{3+} ion at the $^4I_{11/2}$ state and raising it to the $^4F_{7/2}$ state. The process can be expressed as $^4I_{11/2}$+$^4I_{11/2}$ $\rightarrow ^4I_{15/2}$+$^4F_{7/2}$. The following multi-phonon relaxation from the $^4F_{7/2}$ state populates the $^4S_{3/2}$ or $^2H_{11/2}$ level. Once the $^4S_{3/2}$ or $^2H_{11/2}$ level is excited, the radiative transition from $^4S_{3/2}$/ $^2H_{11/2}$ to the ground realizes the green emission.

The emission at 646 nm is performed by the radiative transition of $^4F_{9/2}$ $\rightarrow ^4I_{15/2}$. This means that the 646-nm emission relies on the population of the $^4F_{9/2}$ level. The multi-phonon relaxation from the $^4S_{3/2}$ level is a possible route to populate the $^4F_{9/2}$ level. However, more than five phonons are required in the multi-phonon relaxation process between the $^4S_{3/2}$ and $^4F_{9/2}$ levels[20]. Thus, the population of the $^4F_{9/2}$ level by this mechanism is very small according to the multi-phonon relaxation theory[24]. The main pathways that richly populate the $^4F_{9/2}$ level may be ascribed to the ETU process: $^4F_{7/2}$ + $^4I_{11/2}$ $\rightarrow ^4F_{9/2}$+$^4F_{9/2}$[18].

Under 532-nm excitation, the ions are excited to the intermediate $^4S_{3/2}$ state. Then, one ion in the $^4S_{3/2}$ state returns to the $^4I_{9/2}$ state and transfers its energy to the neighboring ion in the same state, exciting it to the upper the $^2G_{9/2}$ state. The ETU process can be described as $^4S_{3/2}$+$^4S_{3/2}$ $\rightarrow ^4I_{9/2}$+$^2G_{9/2}$. The emission bands centered at 410 and 850 nm are obtained (see Fig. 3(b)), which correspond to the following transitions of Er^{3+}: $^2G_{9/2}$ $\rightarrow ^4I_{15/2}$ and $^4I_{9/2}$ $\rightarrow ^4I_{15/2}$, respectively, indicating that the ETU process is the ideal method in performing the 410-nm upconverting emission. To our knowledge,

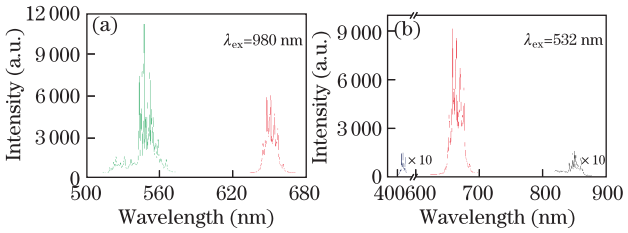

Fig. 3. (Color online) Emission spectra of $Y_{0.55}AlO_3$:5 mol% Er^{3+} x mol% Gd^{3+} under excitations of (a) 980 and (b) 532 nm.

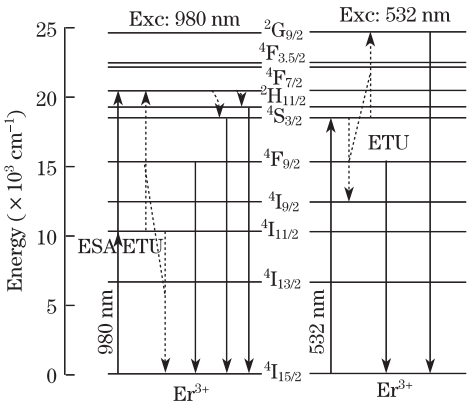

Fig. 4. (Color online) Energy level diagram of Er^{3+} ions and upconversion mechanisms under excitations at 980 and 532 nm.

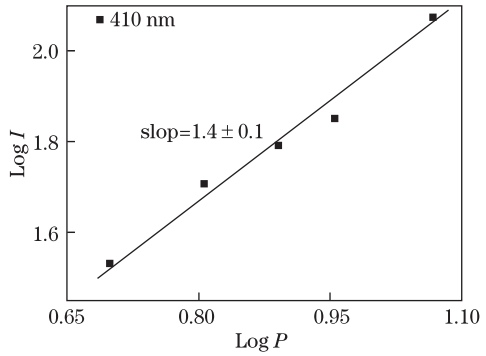

Fig. 5. Double-logarithmic plot of excitation power dependence of upconversion luminescence (410 nm) intensity under 532-nm excitation.

this is the first time that upconversion at 410-nm excited by the 532-nm laser is reported in $YAlO_3$:Er^{3+}. To understand the energy upconversion phenomena, the intensity dependence of upconverted luminescence on excitation power is measured, and the result is shown in Fig. 5. The upconversion intensity I is proportional to the nth power of the excitation intensity P, that is, $I = P^n$, where n represents the number of photons absorbed per upconversion emission[25]. The output slope for the 410-nm emission band is 1.4 which exhibits obvious deviation from 2. As discussed by Pollnau *et al.*[26,27], by increasing the pump power, the energy transfer process can dominate over the linear decay to facilitate the deletion of intermediate excited states; in turn, this leads to a significant reduction of the slope value. For higher rare earth concentration, similarly, the energy transfer rate also increases due to the shortened distance among the rare earth ions even at low pumping power. This may also lead to the deletion of the intermediate excited states, resulting in a reduction of the slope value[28]. In our work, the doped Er^{3+} concentration is 5%. Therefore, the energy transfer process $^4S_{3/2}$+$^4I_{15/2}$ →$^4I_{15/2}$+$^4F_{9/2}$ might also be the dominant depletion mechanism of the intermediate level $^4S_{3/2}$, resulting in a slope of emission intensity of less than 2 versus the excitation power.

Figure 6(a) shows the intensity of green and red emissions as a function of the concentration of Gd^{3+} (x) under 980-nm excitation at the same excitation power. The integrated intensities of green and red emissions first increased and then decreased with the increase of Gd^{3+} content; the maximun intensity existing at $x = 40\%$. The intensity of the green upconversion luminescence of $YAlO_3$:5 mol% Er^{3+} doped with 40 mol% Gd^{3+} is enhanced by about 10 times, and that of the red emission is increased by 8 times compared with the un-doped sample. Similarly, under 532-nm excitation, the intensity of upconversion luminescence of $YAlO_3$:Er^{3+} first increased and then decreased with an increase of Gd^{3+} concentration (see Fig. 6(b)). The upconversion emission at 410 nm of the $YAlO_3$:5 mol% Er^{3+} co-doped with 40 mol% Gd^{3+} is about 7 times higher than that without Gd^{3+} doping. The maximum upconversion intensity under 532-nm excitation also exists at $x = 40\%$. The results show that the upconversion of $YAlO_3$:Er^{3+} can be enhanced effectively with the introduction of the Gd^{3+} ions. Moreover, the maximum upconversion enhancement at Gd^{3+} concentration of 40% whether excited by 980 or 532 nm. It can be understood by the following consideration.

When Gd^{3+} ion (with radius 0.1193 nm) is doped into the $YAlO_3$:5 mol% Er^{3+} samples, Y^{3+} ion (with radius 0.1159 nm) is substituted by Gd^{3+}, thus inducing the expansion of host lattice (see Fig. 1(b)). As the value of electronegative of Y^{3+} is smaller than that of Gd^{3+}, the electronegative difference in $Y_{0.95}Er_{0.05}AlO_3$ is bigger than that in $Y_{0.95-x}Gd_xEr_{0.05}AlO_3$. Thus, the ionicity of Gd–O is smaller than that of Y-O[29]. The Gd^{3+} ions may occupy the sites beside the Er^{3+} activator, distorting the local symmetry of the crystal field around Er^{3+}. The emission of Er^{3+}-doped materials is attributed to the f-f transitions of Er^{3+} ion, and the transition probabilities governing various intra-4f shell transitions of the Er^{3+} ions can be increased by the distortion of the local symmetry around Er^{3+}.

To explore the change of the local environment, the intensity ratio of the $^4S_{3/2}$ →$^4I_{15/2}$ transition to the $^2H_{11/2}$ →$^4I_{15/2}$ under the same 980-nm excitation is carefully calculated (see Fig. 7). The intensity ratio increases with increasing Gd^{3+} concentration from $x = 0$ to 0.4, and then decreases at higher Gd^{3+} concentration. It means that the Gd^{3+} concentration can lead to the change of the radiative transition probability of Er^{3+}. Generally, a quasi-thermal equilibrium occurs between the $^2H_{11/2}$ and $^4S_{3/2}$ levels[30]. With the thermalization of population at the two levels, and ignoring the effects of self-absorption of the luminescence, the intensity ratio of the $^4S_{3/2}$ →$^4I_{15/2}$ transition to the $^2H_{11/2}$ →$^4I_{15/2}$ can be expressed as

$$R = \left[\frac{g_2 A_2 h\nu_2}{g_1 A_1 h\nu_1} \exp\left(-\frac{\Delta E}{kT}\right)\right]^{-1}, \qquad (1)$$

where A_2 and A_1 are the spontaneous emission rates of the $^2H_{11/2}$ and $^4S_{3/2}$ levels, respectively; g_2 and g_1 are

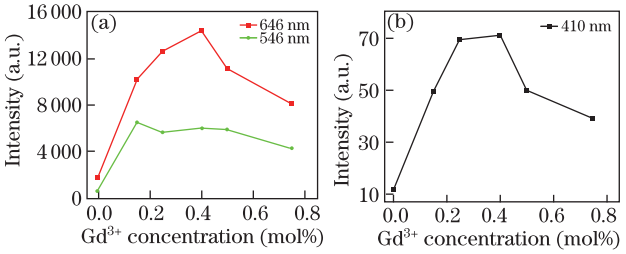

Fig. 6. Effect of Gd^{3+} concentration on the intensity of green and red luminescences $YAlO_3$:Er^{3+} phosphor under (a) 980- and (b) 532-nm excitations.

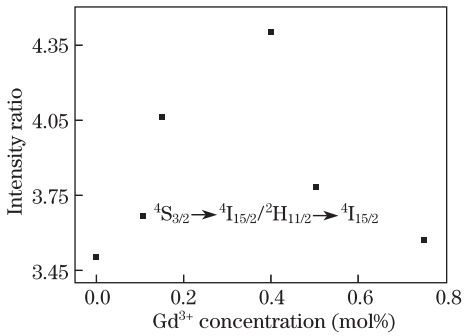

Fig. 7. Intensity ratio as function of Gd^{3+} concentration.

degeneracies $(2J+1)$ of the $^2H_{11/2}$ and $^4S_{3/2}$ levels, respectively; $h\nu_2$ and $h\nu_1$ are the phonon energies of the $^2H_{11/2} \rightarrow {}^4I_{15/2}$ and $^4S_{3/2} \rightarrow {}^4I_{15/2}$ transitions, respectively; ΔE stands for the energy gap between the $^2H_{11/2}$ and $^4S_{3/2}$ levels; k represents the Boltzmann constant; T is the absolute temperature.

In terms of Ref. [31], the emissions in the 545–520 and 570–546 nm regions may be ascribed to the $^2H_{11/2} \rightarrow {}^4I_{15/2}$ and $^4S_{3/2} \rightarrow {}^4I_{15/2}$ transitions, respectively. Considering that the emission peak is hardly shifted with the increase of Gd^{3+} concentration, ΔE can be taken as a constant. Thus, by using the Judd–Ofelt theory[32], the luminescence intensity ratio between the $^2H_{11/2} \rightarrow {}^4I_{15/2}$ and $^4S_{3/2} \rightarrow {}^4I_{15/2}$ transitions (R) can be expressed as

$$R = \mu \frac{0.2285}{0.7056(\Omega_2/\Omega_6) + 0.4109(\Omega_4/\Omega_6) + 0.0870}, \quad (2)$$

where μ is a constant determined by the spectrometer system, and Ω_2, Ω_4, and Ω_6 are the Judd–Ofelt phenomenological parameters.

The hypersensitive transition $^2H_{11/2} \rightarrow {}^4I_{15/2}$, which is related to the Judd–Ofelt phenomenological parameter Ω_2[33], is more sensitive to the local environment. This means that the Ω_2 parameter tends to change more evidently than Ω_4 and Ω_6 with the increase of Gd^{3+} concentration. Therefore, the enhancement of intensity of $YAlO_3$:Er^{3+} by Gd^{3+} doping might be ascribed to the distorted local symmetry of the crystal field around Er^{3+}.

However, the intensity of green and red emissions gradually decreases with the content of Gd^{3+} exceeding 40%. In fact, when the Gd^{3+} content is high enough, the Gd^{3+} ions symmetrically distribute around the Er^{3+} ions as the next nearest neighbor ions. This may restore the symmetry of Er^{3+} ions and is disadvantageous to the f-f transition of Er^{3+}. As a result, the upconversion intensity weakens at high Gd^{3+} concentration.

In conclusion, the upconversion luminescence of $YAlO_3$:Er^{3+} phosphor doping with Gd^{3+} under 980- and 532-nm excitations of diode lasers is studied in this letter. With the introduction of Gd^{3+}, the green and red upconversions pumped by 980 nm and near ultraviolet upconversion emission excited by 532 nm show drastic enhancement. The enhancement of upconversion is due to the distortion of the local symmetry of Er^{3+}. The results indicate that co-doping with Gd^{3+} is a valid method for increasing the efficiency of the upconversion luminescence of $YAlO_3$: Er^{3+}.

This work was supported by the Scientific Research Fund of Hunan Provincial Education Department (Nos. 10A120 and 11B117) and the Hunan Provincial Natural Science Foundation of China (No. 10JJ6012).

References

1. E. Downing, L. Hesselink, J. Ralston, and R. Macfarlane, Science **273,** 1185 (1996).
2. S. Sivakumar, F. C. J. M. van Veggel, and M. Raudsepp, J. Am. Chem. Soc. **127,** 12464 (2005).
3. G. Yi, H. Lu, S. Zhao, Y. Ge, W. Yang, D. Chen, and L. Guo, Nano Lett. **4,** 2191 (2004).
4. H. Yang, Z. Dai, and N. Zu, Chin. Phys. **16,** 1650 (2007).
5. X. Wang, X. Yan, and C. Kan, J. Mater. Chem. **21,** 4251 (2011).
6. H. Yu, L. Zhao, J. Meng, Q. Liang, X. Yu, B. Tang, and J. Xu, Chin. Opt. Lett. **3,** 469 (2005).
7. B. Chen, S. Zhao, and L. Hu, Chin. Opt. Lett. **1,** 699 (2003).
8. C. Li, C. Song, S. Li, and J. Gao, Chin. Opt. Lett. **1,** 664 (2003).
9. S. Zhao, F. Zheng, S. Xu, H. Wang, and B. Wang, Chin. Opt. Lett. **7,** 416 (2008).
10. H. Yang, Z. Dai, and Z. Sun, J. Lumin. **124,** 207 (2007).
11. Y. Wang, Y. Bai, and Y. Song, Chin. Opt. Lett. **7,** 524 (2008).
12. K. W. Krämer, D. Biner, G. Frei, H. U. Güdel, M. P. Hehlen, and S. R. Lüthi, Chem. Mater. **16,** 1244 (2004).
13. F. Auzel, Chem. Rev. **104,** 139 (2004).
14. J. F. Suyver, J. Grimm, M. K. van Veen, D. Biner, K. W. Krämer, and H. U. Güdel, J. Lumin. **117,** 1 (2006).
15. H. Yang, Z. Dai, and Z. Sun, Chin. Phys. **15,** 1273 (2006).
16. H. Xu and Z. Jiang, Chem. Phys. **287,** 155 (2003).
17. R. Francini, S. Pietrantoni, M. Zambelli, A. Speghini, and M. Bettinelli, J. Alloys Compd. **380,** 34 (2004).
18. S. Xiao, X. Yang, Z. Liu, and X. Yan, Opt. Mater. **28,** 285 (2006).
19. H. Liang, Y. Zheng, G. Chen, L. Wu, Z. Zhang, and W. Cao, J. Alloys Compd. **509,** 409 (2011).
20. A. Patra, C. S. Friend, R. Kapoor, and P. N. Prasad, J. Phys. Chem. B **106,** 1909 (2002).
21. G. Wang, S. Dai, J. Zhang, L. Wen, J. Yang, and Z. Jiang, Spectrochim. Acta Part A **64,** 349 (2005).
22. L. Vegard, Z. Phys. **5,** 17 (1921).
23. S. Schnell, W. Ltithy, and H. P. Weber, Journal of Applied Mathematics and Physics **39,** 96 (1988).
24. M. D. Shinn, W. A. Sibley, M. G. Drexhage, and R. N. Brown, Phys. Rev. B **27,** 6635 (1983).
25. A. Bednarkiewicz and W. Strek, J. Phys. D: Appl. Phys. **35,** 2503 (2002).
26. M. Pollnau, D. R. Gamelin, S. R. Luthi, H. U. Güdel, and M. P. Hehlen, Phys. Rev. B **61,** 3337 (2000).
27. J. F. Suyver, A. Aebischer, S. Garcia-Revilla, D. Gerner, and H. U. Güdel, Phys. Rev. B **71,** 125123 (2005).
28. S. Xiao, X. Yang, and J. Ding, Acta Physica Sinica **58,** 3812 (2009).
29. Y. Wang and X. Li, Journal of the Electrochemical Society **153,** G238 (2006).
30. M. D. Shinn, W. A. Sibley, M. G. Drexhage, and R. N. Brown, Phys. Rev. B **27,** 6635 (1983).
31. P. Kisliuk, W. F. Krupke, and J. B. Gruber, J. Chem. Phys. **40,** 3606 (1964).
32. M. J. Weber, Phys. Rev. **157,** 262 (1967).
33. O. Guillot-Noel, B. Bellamy, B. Viana, and D. Gourier, Phys. Rev. B **60,** 1668 (1999).